The MAVIS Image Simulator: predicting the astrometric performance of MAVIS

Stephanie Monty[a], François Rigaut[a], Richard McDermid[b], Jesse Cranney[a], Guido Agapito[c], Cedric Plantet[c], Davide Greggio[d], J. Trevor Mendel[a], Mojtaba Taheri[e], Daniele Vassallo[c], Christian Schwab[b], Giuliana Fiorentino[f], Giuseppe Bono[f], and Dionne Haynes[a]

[a]AAO-Stromlo/AITC, Australian National University, Cotter Road, Weston Creek, ACT 2611, Australia

[b]AAO-Macquarie, 105 Delhi Rd, North Ryde NSW 2113, Australia

[c]INAF – Osservatorio Astronomico di Arcetri, Largo Enrico Fermi 5, I-50125 Firenze, Italy

[d]INAF – Padova, via Francesco Marzolo 8, I-35121 Padova, Italy

[e]Physics & Astronomy Department, University of Victoria, 3800 Finnerty Rd, Victoria, B.C., Canada, V8P 5C2

[f]INAF - Osservatorio Astronomico di Roma, via Frascati 33, I-00078 Monte Porzio Catone, Roma, Italy

ABSTRACT

We present initial results from the Multi-conjugate Adaptive-optics Visible Imager-Spectrograph Image Simulator (MAVISIM) to explore the astrometric capabilities of the next generation instrument MAVIS. A core scientific and operational requirement of MAVIS will be to achieve highly accurate differential astrometry, with accuracies on the order that of the extremely large telescopes. To better understand the impact of known and anticipated astrometric error terms, we have created an initial astrometric budget which we present here to motivate the creation of MAVISIM. In this first version of MAVISIM we include three major astrometric error sources; point spread function (PSF) field variability due to high order aberrations, PSF degradation and field variability due to tip-tilt residual error, and field distortions due to non-common path aberrations in the AO module. An overview of MAVISIM is provided along with initial results from a study using MAVISIM to simulate an image of a Milky Way-like globular cluster. Astrometric accuracies are extracted using PSF-fitting photometry with encouraging results that suggest MAVIS will deliver accuracies of 150μas down to faint magnitudes.

Keywords: Astrometry, Multi-Conjugate Adaptive Optics, Adaptive Optics

1. INTRODUCTION

The first ever multi-conjugate adaptive optics (MCAO) system to operate in the visible, MAVIS is being designed for the Very Large Telescope (VLT) Adaptive Optics Facility (AOF)[1] with the goal of being both a general-purpose instrument, and to provide complimentary to the MAORY/MICADO[2,3] near-IR MCAO system and imager. Correcting light across the wavelength range of 370-950 nm, the MAVIS AO module (AOM) will feed both a 4k×4k imager and integral field spectrograph with four resolution modes.[4] Once on-sky, MAVIS will make the VLT the only 8m-class, near-diffraction limited optical telescope operating on the ground or in space. To do this, MAVIS will use three deformable mirrors conjugated to correct the ground layer, 6 km and 12.5 km layer turbulence, eight laser guide stars (LGS) and three natural guide stars (NGS) to correct a $30'' \times 30''$ FoV.[5] The proposed science cases are remarkably well rounded, ranging from solar system science to studying galaxies at redshit $z \sim 7$ to probe the epoch of re-ionization.[6] One area of astronomy that exploits both the wide-field correction provided by MCAO and the near-diffraction limited, high resolution PSF, is astrometry. As such, a core science capability of MAVIS and an instrumental requirement is achieving highly accurate differential

Further author information: (Send correspondence to S.Monty)
S.Monty: E-mail: Stephanie.Monty@anu.edu.au

astrometry. Formally, MAVIS must achieve astrometric accuracies of 150 μas (with the goal of 50 μas) for high signal-to-noise sources (> 200) separated by no more than one arcsecond. Furthermore, this requirement assumes that a reference source is present in the image and that the lower order plate scale and rotational terms can be calibrated to within 0.01%. To verify this requirement is achievable, we have begun work on a MAVIS astrometric error budget similar to the the work done by TMT/NFIRAOS[7] and EELT/MAORY.[8] To aid in building the budget, we have developed MAVISIM, a tool to create realistic MAVIS images by accounting for major sources of astrometic error. In the current version of MAVISIM we account for three major sources of astrometric error. Here we present preliminary results from MAVISIM, highlighting the predicted astrometric capabilities of MAVIS after modeling three dominant error terms.

2. ASTROMETRIC ERROR TERMS

During Phase A of the MAVIS design process, a preliminary astrometric budget was compiled which included both known and potential astrometric error sources for MCAO systems. As stated, much inspiration was drawn from the work of TMT/NFIRAOS and ELT/MAORY. In this section we list the astrometric error terms the MAVIS team is currently considering and provide a brief description of how we are considering each.

2.1 Preliminary Astrometric Budget

Thus far we have identified six astrometric error sources to be considered in the MAVIS error budget. Additionally, we have chosen to consider our method for astrometric calibration simultaneously to assess our ability to accommodate and correct for many of the error terms. The major error sources identified thus far are listed in Table 1 alongside our proposed plan to study each, and whether the error has been considered in the current study (MAVISIM 1.0). Referring to Table 1, high order and low order aberrations are denoted as HO and LO respectively and non-common path aberrations as NCPAs. The term "end-to-end AO simulation" is used to denote simulations of the MAVIS AO loop made in YAO,[9] PASSATA[10,11] or COMPASS.[12] Note that the budget is very preliminary and input from the community would be appreciated.

2.2 Modeled Terms in MAVISIM 1.0

Inspired by the MICADO image simulator SimCADO,[13] we have built MAVISIM to simulate the expected imaging capabilities of MAVIS with the ultimate goal of testing and refining potential science cases*. Currently, MAVISIM is being used primarily to aid in the construction of the astrometric budget and to probe science cases related to resolved stellar populations.[6] In this first version of MAVISIM we account for three major sources of astrometric error and model real detector and observational characteristics.

2.2.1 PSF field variability: LGS Anisoplanatism

The first error term we have considered is the effect of uncorrected high order aberrations associated primarily with LGS anisoplanatism. The anisoplanatic error captures the disagreement in turbulence profiles between an AO reference source and science object. As the angular separation between a science object and AO reference source increases, the shared turbulence volume along the line of sight decreases. This decrease results in the reconstructed turbulent phase being a poorer representation of the true phase, thus worsening the AO correction.[19] Because of the angular dependence, the LGS anisoplanatic error varies across the field of view (FoV) reflecting the LGS constellation geometry. To capture the field variability we have generated a database of PSFs across the MAVIS FoV. The PSFs are generated using an implementation of the Fourier method which uses the Power Spectral Density of the turbulence to recover the long exposure (time averaged) PSF.[11,20,21] In Fig. 1 we show a MAVISIM image of a crowded stellar field to highlight the treatment of PSF spatial variability.

*We rely heavily on the NumPy,[14] SciPy,[15] Astropy[16,17] and Matplotlib[18] Python libraries in MAVISIM.

Table 1. Preliminary astrometric error budget for MAVIS. Errors are classified generally with specific

Error Source	**Investigation Strategy**	**Incl.**
PSF Shape		
1. HO Aberrations	MAVSIM: long exposure PSF and end-to-end PSF	✓
2. LO Aberrations	MAVISIM: apply tip-tilt residual map from end-to-end AO simulations	✓
Atmospheric Effects		
1. Distortion	End-to-end AO simulation	✗
2. Chromatic Dispersion	MAVISIM: create broadband PSF using distortion values from Zemax end-to-end simulation	✗
Detector Characteristics		
1. Charge Diffusion	Resolved: assumed fixed effect, 0.94×pixel size	✓
2. Quantum Efficiency Variations	Detector characterisation in the lab	✗
3. Pixel Size	Resolved: Assuming Nyquist sampling at 550 nm	✓
3. Photon & Read Noise	Assumed for preliminary detector choice	✓
AOM Optical NCPAs		
1. Static Distortion (e.g. polish. errors)	MAVISIM: apply distortion map determined from Zemax end-to-end simulations	✓
2. Dynamic Distortion (e.g. flexure)	MAVISIM: simulate expected distortion by perturbing optical elements and recreating static maps[8]	✗
AOM Deformable Mirror NCPAs		
1. Dynamic (e.g. actuator failure)	End-to-end AO simulation	✗
VLT NCPAs		
1. Static (e.g. polish. errors)	MAVISIM: use archival data?	✗
2. Dynamic (e.g. from M1, M2, M3)	End-to-end AO simulations: phase screens to represent mirrors	✗
Calibration		
1. Pinhole Mask	MAVISIM: simulate the mask characteristics needed to recover the static AOM distortion map	✗

2.2.2 Tip-tilt residual

The second error we have modeled thus far, is the tip-tilt (TT) residual resulting from the incomplete correction of lower order aberrations. We model the TT residual as the sum of the tomographic, vibrational and measurement errors. The tomographic error includes NGS anisoplanatism. To examine the effect of the TT residual on different science cases, we consider several NGS constellations to recover maps of the TT residual across the MAVIS FoV.[11] The maps vary the NGS distance from the centre of the MAVIS FoV, individual NGS brightness and NGS constellation geometry. We model the residual as a 2D multivariate Gaussian kernel that captures both the magnitude and variability as a function of position in the field.

2.2.3 Static distortion

The final astrometric error we model in this first version of MAVISIM is static distortion resulting from the opto-mechanics of the AOM.[22] To recover the static distortion map of the AOM we use an end-to-end approach in Zemax. At the moment we only consider the static terms present in the AOM and do not consider any

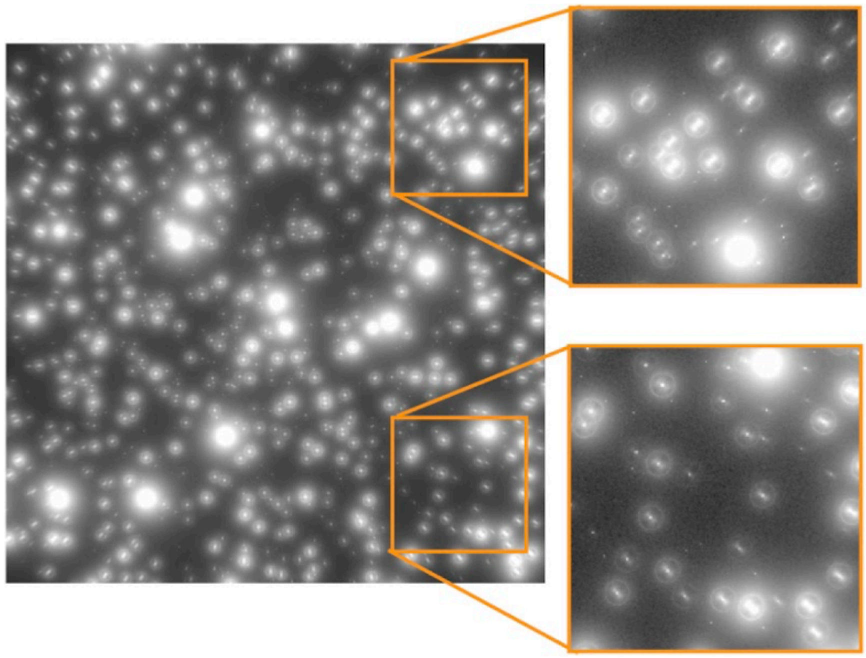

Figure 1. Simulated log-intensity image created using MAVISIM of a globular cluster at a distance of 5 kpc. The spatial variability of the PSF across the FoV is highlighted with the zoomed insets to show the treatment of higher order aberrations by MAVISIM, specifically LGS anisoplanatism as discussed in Section 2.2.1.

dynamic terms (e.g. telescope vibrations). The static distortion is largely dominated by NCPAs in the AOM, although polishing errors are not considered at this time. The MAVIS AOM is unique among MCAO systems as it makes use of transmissive, on-axis optics, largely reducing NCPAs within the system. In the current version of the distortion map the distortion introduced is incredibly small, with a maximum value of ~ 0.15 mas at the edge of the MAVIS corrected FoV (a circle radius 15”).

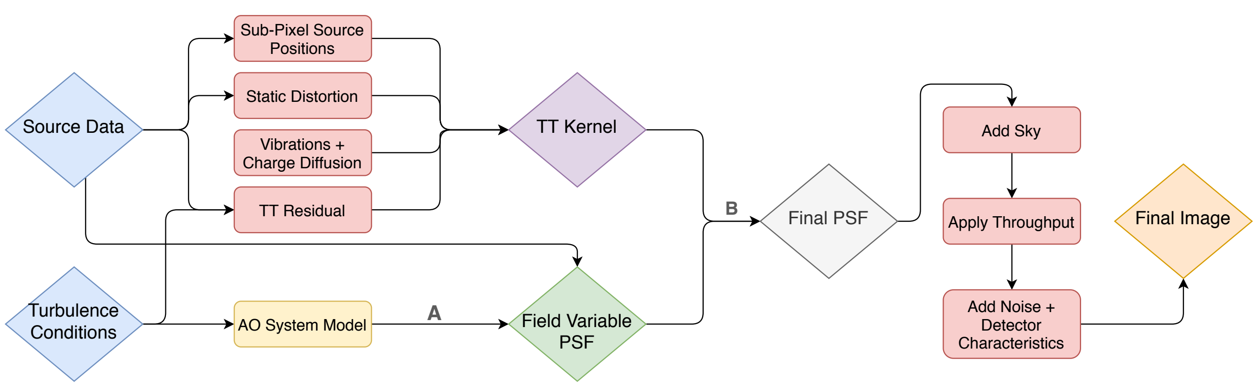

Figure 2. Flowdown chart representing the creation of an image in MAVISIM. Point “A” represents the Fourier transform used to create the database of field variable PSFs. Point “B” represents the convolution used to create the final PSF that captures both the high and low order terms for each object.

3. IMAGE GENERATION

A flowdown chart of the process for image creation using MAVISIM is given in Fig. 2. A brief description of the process will be given here, for a more complete description of MAVISIM the reader is directed to our upcoming paper (Monty et al. in prep. for MNRAS). The process of image generation begins with an input source catalogue of (x,y) positions and flux. At the moment we only consider point sources. The catalogue information is then used to recover the static distortion and TT residual for each object (depending on it's position in the field). This is combined with an additional vibration and charge diffusion term[23] to create the final TT kernel for each object. The object's position is also used to recover a spatially-dependent Fourier PSF from the database using a Bilinear interpolation. Point "A" on the diagram represents the Fourier transform used to create the Fourier PSF. The Fourier PSF is then convolved with the object TT kernel at point "B" to create the final PSF for each object. The process to create the final image of a single object is then depicted with the addition of the sky background, throughput considerations of both the VLT and MAVIS AOM and noise characteristics of the detector.

4. PRELIMINARY ASTROMETRIC ACCURACY

As a preliminary exploration of the MAVIS astrometric capabilities, we have fed MAVISIM a catalogue of a crowded stellar field, generated an image and used PSF-fitting photometry to recover stellar positions. These positions were then compared against the input positions to estimate the astrometric accuracy. The input catalogue used for the study is an analogue to the Milky Way globular cluster NGC 3201.[24] To perform the PSF-fitting photometry we used DAOPHOT/ALLSTAR,[25,26] a well-tested, successful tool that has been used many times to analyse MCAO data. We largely followed the methodology laid out in Monty et al., 2018 with small changes to accommodate the higher strehl ratio of the MAVIS PSF.[27] As NGC 3201 is a bright and nearby cluster, we used the best NGS constellation to generate the TT residual map. The constellation consists of three magnitude 15 stars (in H band) located symmetrically throughout the field at a distance of ten arcseconds (radially) from the centre of the FoV.

Initial results from this study are shown in Fig. 3 where we show the astrometric accuracy as a function of magnitude for a monochromatic (550 nm) image integrated for 30s. Note that the magnitudes are taken directly from the input catalogue and are thus the ground truth V band magnitudes calibrated to the Vega magnitude system. The left plot of Fig. 3 shows the individual measured stellar accuracies. Stars with accuracies of 150 μas (requirement) or better are plotted as the dark cyan dots, while stars with accuracies of 50 μas (goal) are plotted as the turquoise dots. For reference, $\sim$ 30% of the recovered stars had accuracies of 50 μas or better while $\sim$ 60% of the recovered stars had accuracies of 150 μas or better. The right plot in Fig. 3 shows the astrometric dispersion as a function of mean magnitude created by sliding a window size 30 across the measured magnitudes. The shaded region bounds 150 μas or better. The results are encouraging as the dispersion remains small down to faint magnitudes ($\sim$ 23) considering we have modeled three of the major astrometric error terms. The results are also encouraging in the context of being able to model and perform PSF-fitting photometry on the MAVIS PSF, bearing in mind that the Fourier PSF is idealised.

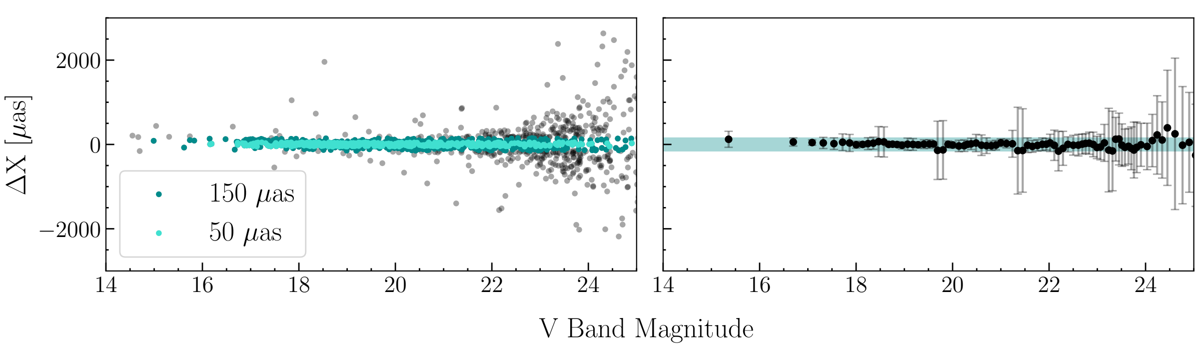

Figure 3. Preliminary astrometric accuracies (the difference between the input and recovered x positions) as a function of input magnitude for a monochromatic image (550 nm) integrated for 30s. The left plot shows the accuracies of individual stars with stars having astrometric accuracies of 150 μas or better marked in dark cyan and stars with accuracies of 50 μas or better marked in turquoise. The right plot shows the astrometric dispersion as a function of mean magnitude created using a sliding window of size 30.

5. CONCLUSIONS

We have begun building an astrometric budget for the next generation VLT instrument MAVIS. To aid in the creation of the budget and to verify (as well as can be done prior to going on-sky) that MAVIS will meet the challenging astrometric requirement of 150 μas (goal of 50 μas)[†], we have built a MAVIS image simulator. In this current version of MAVISIM we have accounted for three major sources of astrometric error; PSF field variability associated largely with LGS anisoplanatism, TT residuals related the NGS constellation characteristics and static distortion from the AOM. Ultimately we plan on incorporating as many of the astrometric error sources identified in Table 1 as possible in MAVISIM. We have presented preliminary results from MAVISIM in a crowded stellar field showing that MAVIS will achieve astrometric accuracies of 150 μas or better down to relatively faint magnitudes. Further applications of MAVISIM and updated results will be showcased in our upcoming paper (Monty et al. in prep for MNRAS.) MAVIS is a challenging and ambitious project and understanding the full astrometric capabilities of the instrument is a challenge in of itself. We are only just beginning to explore what MAVIS will be capable of and it is truly an exciting time to be a part of the team.

ACKNOWLEDGMENTS

SM wishes to acknowledge and celebrate the First Australians on whose lands the Australian National University operates, and pay her respect to the elders of the Ngambri and Ngunnawal people, past, present, and emergent.

SM also acknowledges the support of the Natural Sciences and Engineering Research Council of Canada (NSERC). Nous remercions le Conseil de recherches en sciences naturelles et en génie du Canada (CRSNG) de son soutien.

REFERENCES

[1] Arsenault, R., Madec, P.-Y., Paufique, J., La Penna, P., Stroebele, S., Vernet, E., Pirard, J.-F., Hackenberg, W., Kuntschner, H., Jochum, L., Kolb, J., Muller, N., Le Louarn, M., Amico, P., Hubin, N., Lizon, J.-L., Ridings, R., Abad, J. A., Fischer, G., Heinz, V., Kiekebusch, M., Argomedo, J., Conzelmann, R., Tordo, S., Donaldson, R., Soenke, C., Duhoux, P., Fedrigo, E., Delabre, B., Jost, A., Duchateau, M., Downing, M., Moreno, J. R., Dorn, R., Manescau, A., Bonaccini Calia, D., Quattri, M., Dupuy, C., Guidolin, I. M., Comin, M., Guzman, R., Buzzoni, B., Quentin, J., Lewis, S., Jolley, P., Kraus, M., Pfrommer, T., Biasi, R., Gallieni, D., Bechet, C., and Stuik, R., "ESO adaptive optics facility progress report," in [*Adaptive Optics Systems III*], Ellerbroek, B. L., Marchetti, E., and Véran, J.-P., eds., *Society of Photo-Optical Instrumentation Engineers (SPIE) Conference Series* **8447**, 84470J (July 2012).

[2] Diolaiti, E., Ciliegi, P., Abicca, R., Agapito, G., Arcidiacono, C., Baruffolo, A., Bellazzini, M., Biliotti, V., Bonaglia, M., Bregoli, G., Briguglio, R., Brissaud, O., Busoni, L., Carbonaro, L., Carlotti, A., Cascone, E., Correia, J. J., Cortecchia, F., Cosentino, G., De Caprio, V., de Pascale, M., De Rosa, A., Del Vecchio, C., Delboulbé, A., Di Rico, G., Esposito, S., Fantinel, D., Feautrier, P., Felini, C., Ferruzzi, D., Fini, L., Fiorentino, G., Foppiani, I., Ghigo, M., Giordano, C., Giro, E., Gluck, L., Hénault, F., Jocou, L., Kerber, F., La Penna, P., Lafrasse, S., Lauria, M., le Coarer, E., Le Louarn, M., Lombini, M., Magnard, Y., Maiorano, E., Mannucci, F., Mapelli, M., Marchetti, E., Maurel, D., Michaud, L., Morgante, G., Moulin, T., Oberti, S., Pareschi, G., Patti, M., Puglisi, A., Rabou, P., Ragazzoni, R., Ramsay, S., Riccardi, A., Ricciardi, S., Riva, M., Rochat, S., Roussel, F., Roux, A., Salasnich, B., Saracco, P., Schreiber, L., Spavone, M., Stadler, E., Sztefek, M. H., Ventura, N., Vérinaud, C., Xompero, M., Fontana, A., and Zerbi, F. M., "MAORY: adaptive optics module for the E-ELT," in [*Adaptive Optics Systems V*], Marchetti, E., Close, L. M., and Véran, J.-P., eds., *Society of Photo-Optical Instrumentation Engineers (SPIE) Conference Series* **9909**, 99092D (July 2016).

[3] Davies, R., Ageorges, N., Barl, L., Bedin, L. R., Bender, R., Bernardi, P., Chapron, F., Clenet, Y., Deep, A., Deul, E., Drost, M., Eisenhauer, F., Falomo, R., Fiorentino, G., Förster Schreiber, N. M., Gendron, E., Genzel, R., Gratadour, D., Greggio, L., Grupp, F., Held, E., Herbst, T., Hess, H. J., Hubert, Z., Jahnke, K., Kuijken, K., Lutz, D., Magrin, D., Muschielok, B., Navarro, R., Noyola, E., Paumard, T., Piotto, G., Ragazzoni, R., Renzini, A., Rousset, G., Rix, H. W., Saglia, R., Tacconi, L., Thiel, M., Tolstoy, E., Trippe,

[†]Note that the complete requirement is stated in Section 1

S., Tromp, N., Valentijn, E. A., Verdoes Kleijn, G., and Wegner, M., "MICADO: the E-ELT adaptive optics imaging camera," in [*Ground-based and Airborne Instrumentation for Astronomy III*], McLean, I. S., Ramsay, S. K., and Takami, H., eds., *Society of Photo-Optical Instrumentation Engineers (SPIE) Conference Series* **7735**, 77352A (July 2010).

[4] Ellis, S., McDermid, R., Cresci, G., Schwab, C., Rigaut, F., and et al., "Mavis: science case, imager, and spectrograph," *Proc. SPIE* **11447-285 (this conference)** (2020).

[5] Rigaut, F., McDermid, R., Cresci, G., Viotto, V., Ellis, S., Broderick, D., Agapito, G., Fusco, T., Neichel, B., Haguenauer, P., Plantet, C., Salasnich, B., Aliverti, M., Antoniucci, S., Balestra, A., Baruffolo, A., Bergomi, M., Bonaglia, M., Bono, G., Busoni, L., Carolo, E., Chinellato, S., Content, R., Cranney, J., De Silva, G., Esposito, S., Fantinel, D., Farinato, J., Haynes, D., Horton, A., Gaston, G., Gilbert, J., Gratadour, D., Greggio, D., Gullieuszik, M., Korkiakoski, V., Magrin, D., Magrini, L., Marafatto, L., Mcgregor, H., Mendel, T., Monty, S., Pedichini, F., Pinna, E., Portaluri, E., Radhakrishnan, K., Ragazzoni, R., Robertson, D., Schwab, C., Sharp, R., Stroebele, S., Thorn, E., Vaccarella, A., Vassallo, D., Venkatesan, S., Waller, L., Warner, S., Zamkotsian, F., and Zhang, H., "MAVIS Conceptual Design," in [*(submitted to) Ground-based and Airborne Instrumentation for Astronomy VIII*], International Society for Optics and Photonics, SPIE (2020).

[6] McDermid, R. M., Cresci, G., Rigaut, F., Bouret, J.-C., De Silva, G., Gullieuszik, M., Magrini, L., Mendel, J. T., Antoniucci, S., Bono, G., Kamath, D., Monty, S., Baumgardt, H., Cortese, L., Fisher, D., Mannucci, F., Migliorini, A., Sweet, S., Vanzella, E., Zibetti, S., and White Papers., w. a. c. f. t. a. o. t. M., "Phase A Science Case for MAVIS – The Multi-conjugate Adaptive-optics Visible Imager-Spectrograph for the VLT Adaptive Optics Facility," *arXiv e-prints* , arXiv:2009.09242 (Sept. 2020).

[7] Schöck, M., Andersen, D., Rogers, J., Ellerbroek, B., Chisholm, E., Dunn, J., Herriot, G., Larkin, J., Moore, A., Suzuki, R., Wincentsen, J., and Wright, S., "Flowdown of the TMT astrometry error budget(s) to the IRIS design," in [*Ground-based and Airborne Instrumentation for Astronomy VI*], Evans, C. J., Simard, L., and Takami, H., eds., *Society of Photo-Optical Instrumentation Engineers (SPIE) Conference Series* **9908**, 9908AD (Aug. 2016).

[8] Rodeghiero, G., Pott, J. U., Arcidiacono, C., Massari, D., Glück, M., Riechert, H., and Gendron, E., "The impact of ELT distortions and instabilities on future astrometric observations," *MNRAS* **479**, 1974–1985 (Sept. 2018).

[9] Rigaut, F. and Van Dam, M., "Simulating Astronomical Adaptive Optics Systems Using Yao," in [*Proceedings of the Third AO4ELT Conference*], Esposito, S. and Fini, L., eds., 18 (Dec. 2013).

[10] Agapito, G., Puglisi, A., and Esposito, S., "PASSATA: object oriented numerical simulation software for adaptive optics," in [*Adaptive Optics Systems V*], Marchetti, E., Close, L. M., and Véran, J.-P., eds., *Society of Photo-Optical Instrumentation Engineers (SPIE) Conference Series* **9909**, 99097E (July 2016).

[11] Agapito, G., Vassallo, D., Plantet, C., Viotto, V., Pinna, E., and et al., "Mavis: System modelling and performance prediction," *Proc. SPIE* **11448 (this conference)** (2020).

[12] Gratadour, D., Puech, M., Vérinaud, C., Kestener, P., Gray, M., Petit, C., Brulé, J., Clénet, Y., Ferreira, F., Gendron, E., Lainé, M., Sevin, A., Rousset, G., Hammer, F., Jégouzo, I., Paillous, M., Taburet, S., Yang, Y., Beuzit, J. L., Carlotti, A., Westphal, M., Epinat, B., Ferrari, M., Gautrais, T., Lambert, J. C., Neichel, B., and Rodionov, S., "COMPASS: an efficient, scalable and versatile numerical platform for the development of ELT AO systems," in [*Adaptive Optics Systems IV*], Marchetti, E., Close, L. M., and Veran, J.-P., eds., *Society of Photo-Optical Instrumentation Engineers (SPIE) Conference Series* **9148**, 91486O (Aug. 2014).

[13] Leschinski, K., Czoske, O., Köhler, R., Mach, M., Zeilinger, W., Verdoes Kleijn, G., Alves, J., Kausch, W., and Przybilla, N., "SimCADO: an instrument data simulator package for MICADO at the E-ELT," in [*Modeling, Systems Engineering, and Project Management for Astronomy VI*], Angeli, G. Z. and Dierickx, P., eds., *Society of Photo-Optical Instrumentation Engineers (SPIE) Conference Series* **9911**, 991124 (Aug. 2016).

[14] Harris, C. R., Millman, K. J., van der Walt, S. J., Gommers, R., Virtanen, P., Cournapeau, D., Wieser, E., Taylor, J., Berg, S., Smith, N. J., Kern, R., Picus, M., Hoyer, S., van Kerkwijk, M. H., Brett, M., Haldane, A., del R'ıo, J. F., Wiebe, M., Peterson, P., G'erard-Marchant, P., Sheppard, K., Reddy, T., Weckesser,

W., Abbasi, H., Gohlke, C., and Oliphant, T. E., "Array programming with NumPy," *Nature* **585**, 357–362 (Sept. 2020).

[15] Virtanen, P., Gommers, R., Oliphant, T. E., Haberland, M., Reddy, T., Cournapeau, D., Burovski, E., Peterson, P., Weckesser, W., Bright, J., van der Walt, S. J., Brett, M., Wilson, J., Millman, K. J., Mayorov, N., Nelson, A. R. J., Jones, E., Kern, R., Larson, E., Carey, C. J., Polat, İ., Feng, Y., Moore, E. W., VanderPlas, J., Laxalde, D., Perktold, J., Cimrman, R., Henriksen, I., Quintero, E. A., Harris, C. R., Archibald, A. M., Ribeiro, A. H., Pedregosa, F., van Mulbregt, P., and SciPy 1.0 Contributors, "SciPy 1.0: Fundamental Algorithms for Scientific Computing in Python," *Nature Methods* **17**, 261–272 (2020).

[16] Astropy Collaboration, Robitaille, T. P., Tollerud, E. J., Greenfield, P., Droettboom, M., Bray, E., Aldcroft, T., Davis, M., Ginsburg, A., Price-Whelan, A. M., Kerzendorf, W. E., Conley, A., Crighton, N., Barbary, K., Muna, D., Ferguson, H., Grollier, F., Parikh, M. M., Nair, P. H., Unther, H. M., Deil, C., Woillez, J., Conseil, S., Kramer, R., Turner, J. E. H., Singer, L., Fox, R., Weaver, B. A., Zabalza, V., Edwards, Z. I., Azalee Bostroem, K., Burke, D. J., Casey, A. R., Crawford, S. M., Dencheva, N., Ely, J., Jenness, T., Labrie, K., Lim, P. L., Pierfederici, F., Pontzen, A., Ptak, A., Refsdal, B., and Servillat, M. andz Streicher, O., "Astropy: A community Python package for astronomy," *A&A* **558**, A33 (Oct. 2013).

[17] Astropy Collaboration, Price-Whelan, A. M., SipHocz, B. M., G"unther, H. M., Lim, P. L., Crawford, S. M., Conseil, S., Shupe, D. L., Craig, M. W., Dencheva, N., Ginsburg, A., Vand erPlas, J. T., Bradley, L. D., P'erez-Su'arez, D., de Val-Borro, M., Aldcroft, T. L., Cruz, K. L., Robitaille, T. P., Tollerud, E. J., Ardelean, C., Babej, T., Bach, Y. P., Bachetti, M., Bakanov, A. V., Bamford, S. P., Barentsen, G., Barmby, P., Baumbach, A., Berry, K. L., Biscani, F., Boquien, M., Bostroem, K. A., Bouma, L. G., Brammer, G. B., Bray, E. M., Breytenbach, H., Buddelmeijer, H., Burke, D. J., Calderone, G., Cano Rodr'iguez, J. L., Cara, M., Cardoso, J. V. M., Cheedella, S., Copin, Y., Corrales, L., Crichton, D., D'Avella, D., Deil, C., Depagne, E., Dietrich, J. P., Donath, A., Droettboom, M., Earl, N., Erben, T., Fabbro, S., Ferreira, L. A., Finethy, T., Fox, R. T., Garrison, L. H., Gibbons, S. L. J., Goldstein, D. A., Gommers, R., Greco, J. P., Greenfield, P., Groener, A. M., Grollier, F., Hagen, A., Hirst, P., Homeier, D., Horton, A. J., Hosseinzadeh, G., Hu, L., Hunkeler, J. S., Ivezi'c, Z., Jain, A., Jenness, T., Kanarek, G., Kendrew, S., Kern, N. S., Kerzendorf, W. E., Khvalko, A., King, J., Kirkby, D., Kulkarni, A. M., Kumar, A., Lee, A., Lenz, D., Littlefair, S. P., Ma, Z., Macleod, D. M., Mastropietro, M., McCully, C., Montagnac, S., Morris, B. M., Mueller, M., Mumford, S. J., Muna, D., Murphy, N. A., Nelson, S., Nguyen, G. H., Ninan, J. P., N"othe, M., Ogaz, S., Oh, S., Parejko, J. K., Parley, N., Pascual, S., Patil, R., Patil, A. A., Plunkett, A. L., Prochaska, J. X., Rastogi, T., Reddy Janga, V., Sabater, J., Sakurikar, P., Seifert, M., Sherbert, L. E., Sherwood-Taylor, H., Shih, A. Y., Sick, J., Silbiger, M. T., Singanamalla, S., Singer, L. P., Sladen, P. H., Sooley, K. A., Sornarajah, S., Streicher, O., Teuben, P., Thomas, S. W., Tremblay, G. R., Turner, J. E. H., Terr'on, V., van Kerkwijk, M. H., de la Vega, A., Watkins, L. L., Weaver, B. A., Whitmore, J. B., Woillez, J., Zabalza, V., and Astropy Contributors, "The Astropy Project: Building an Open-science Project and Status of the v2.0 Core Package," *AJ* **156**, 123 (Sept. 2018).

[18] Hunter, J. D., "Matplotlib: A 2d graphics environment," *Computing in Science & Engineering* **9**(3), 90–95 (2007).

[19] Rigaut, F. and Neichel, B., "Multiconjugate Adaptive Optics for Astronomy," *arXiv e-prints* , arXiv:2003.03097 (Mar. 2020).

[20] Roddier, F., "The effects of atmospheric turbulence in optical astronomy," *Progess in Optics* **19**, 281–376 (Jan. 1981).

[21] Jolissaint, L., Véran, J.-P., and Conan, R., "Analytical modeling of adaptive optics: foundations of the phase spatial power spectrum approach," *Journal of the Optical Society of America A* **23**, 382–394 (Feb. 2006).

[22] Greggio, D., Di Filippo, S., Magrin, D., Schwab, C., Viotto, and et al., "Mavis adaptive optics module optical design," *Proc. SPIE* **11448-280 (this conference)** (2020).

[23] Toyozumi, H. and Ashley, M. C. B., "Intra-pixel sensitivity variation and charge transfer inefficiency — results of ccd scans," *PASP* **22**(3), 257–266 (2005).

[24] Baumgardt, H., "N -body modelling of globular clusters: masses, mass-to-light ratios and intermediate-mass black holes," *MNRAS* **464**, 2174–2202 (Jan. 2017).

[25] Stetson, P. B., "DAOPHOT: A Computer Program for Crowded-Field Stellar Photometry," *PASP* **99**, 191 (Mar. 1987).

[26] Stetson, P. B., "The Center of the Core-Cusp Globular Cluster M15: CFHT and HST Observations, ALLFRAME Reductions," *PASP* **106**, 250 (Mar. 1994).

[27] Monty, S., Puzia, T. H., Miller, B. W., Carrasco, E. R., Simunovic, M., Schirmer, M., Stetson, P. B., Cassisi, S., Venn, K. A., Dotter, A., Goudfrooij, P., Perina, S., Pessev, P., Sarajedini, A., and Taylor, M. A., "The GeMS/GSAOI Galactic Globular Cluster Survey (G4CS). I. A Pilot Study of the Stellar Populations in NGC 2298 and NGC 3201," *ApJ* **865**, 160 (Oct. 2018).